


# Variational Tensor Wave Functions for the Interacting Quantum Spin Hall Phase

Yixin Ma, Shenghan Jiang,<sup>\*</sup> and Chao Xu<sup>†</sup>

Kavli Institute for Theoretical Sciences, University of Chinese Academy of Sciences, Beijing 100190, China

 (Received 7 February 2023; revised 19 January 2024; accepted 31 January 2024; published 21 March 2024)

The quantum spin hall (QSH) phase, also known as the 2D topological insulator, is characterized by protected helical edge modes arising from time reversal symmetry. While initially proposed as band insulators, this phase can also manifest in strongly correlated systems where conventional band theory fails. To overcome the challenge of simulating this phase in realistic correlated models, we propose a novel framework utilizing fermionic tensor network states. Our approach involves constructing a tensor representation of the fixed-point wave function based on an exact solvable model, enabling us to derive a set of tensor equations governing the transformation rules of local tensors under symmetry operations. These tensor equations lead to the anomalous edge theory, which provides a comprehensive description of the QSH phase. By solving these tensor equations, we obtain variational ansatz for the QSH phase, which we subsequently verify its topological properties through numerical calculations. This method serves as an initial step toward employing tensor algorithms to simulate the QSH phase in strongly correlated systems, opening new avenues for investigating and understanding topological phenomena in complex materials.

DOI: [10.1103/PhysRevLett.132.126504](https://doi.org/10.1103/PhysRevLett.132.126504)

*Introduction.*—The discovery of the quantum spin Hall (QSH) phase [1] has sparked research interest in studying the interplay between symmetry and topology in quantum materials [2,3]. Initially proposed as a topological band insulator, the QSH phase is characterized by stable properties such as anomalous helical edge modes and topological response to electromagnetic fields [4]. It has been found that the QSH phase can also be realized as a Mott insulator in strongly correlated systems, representing an example of interacting fermionic symmetry-protected topological (SPT) phases [5–18]. Solvable models based on commuting-projector Hamiltonians have been used to construct various interacting fermionic SPT phases, including the QSH phase [19–24]. However, these models only provide fixed-point wave functions and are hardly useful for numerical simulations.

To construct generic variational wave functions beyond the fixed point, we turn to fermionic tensor networks [25–33]. Our strategy is presented as following. Motivated by the interacting edge theory [34,35], we introduce the fixed-point wave function proposed in Ref. [24]. We then translate it to fermionic projected entangled-pair states (fPEPS) representation, from which we derive a set of tensor equations for symmetry actions on tensors. From tensor equations, we obtain algebraic data characterizing the anomalous edge theory of the QSH phase. Finally, we apply our method to a spin-1/2 fermionic system on honeycomb and square lattice: by listing and solving tensor equations, we get variational ansatz for the QSH phase on such systems. We further numerically extract nontrivial many-body topological invariants [36,37] from these variational tensor wave functions.

*The fixed-point wave function.*—The QSH phase hosts charge conservation symmetry  $n_f$  and time reversal symmetry  $\mathcal{T}$ , where

$$\mathcal{T}^2 = \exp[i\pi n_f] \equiv F, \quad \mathcal{T} \cdot n_f \cdot \mathcal{T}^{-1} = n_f, \quad (1)$$

with  $F$  the fermion parity operator.

To gain insight into the interacting bulk wave function, we initiate our exploration by examining its anomalous edge states with interactions. These edge states manifest a succinct representation using bosonization [38], and is described by [34,35] (see Appendix A for details)

$$\begin{aligned} \mathcal{L}_{\text{edge}} = & \frac{1}{2\pi} \partial_x \theta \partial_t \phi - \frac{v_F}{4\pi} \left( \frac{1}{K} (\partial_x \theta)^2 + K (\partial_x \phi)^2 \right) \\ & + \alpha \cos(2\theta - 2\theta_0) + \dots, \end{aligned} \quad (2)$$

where  $\phi$  and  $\theta$  are conjugate fields, taking value in  $[0, 2\pi)$ , and  $K$  is the Luttinger parameter. Symmetry actions on  $\theta$  and  $\phi$  read

$$\begin{aligned} U(\varphi): \quad & \phi \rightarrow \phi + \varphi, \quad \theta \rightarrow \theta; \\ \mathcal{T}: \quad & \phi \rightarrow -\phi, \quad \theta \rightarrow \theta + \pi, \quad i \rightarrow -i, \end{aligned} \quad (3)$$

which constrain possible scattering terms in Eq. (2).

As illustrated in Fig. 1, the anomalous properties of such edge theory become apparent through its topological defects. Specifically, its  $\mathcal{T}$  domain wall, characterized by a  $\pm\pi$  shift in  $\theta$ , carries fractional  $\pm\frac{1}{2}U(1)$  charge [39].

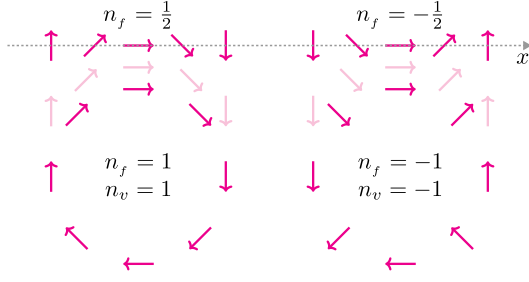


FIG. 1. Edge domain walls and bulk vortices of  $\theta$  field with fermion decoration.

We proceed by extending  $\theta$  to bulk. The  $\pm\pi$  domain wall at edge is identified as  $\pm\frac{1}{2}\theta$  vortex, as shown in Fig. 1. The half-charge at edge domain wall motivates a decorated vortex picture [40,41]: each vortex carries fermion  $n_f = n_v$ , where  $n_v$  is the vorticity. The  $\mathcal{T}$  symmetry can be recovered by proliferating vortices, with  $n_f$  remaining conserved throughout this process due to the conservation of total vorticity.

Equipped with the decorated vortex picture, we introduce the fixed-point wave function [24]. As in Fig. 2, we consider a system with spin-1/2 fermions  $f_\sigma$ 's at a honeycomb lattice, and Ising spins  $|\tau\rangle$ 's at the dual triangular lattice, where  $\sigma, \tau = \uparrow/\downarrow$ .  $\mathcal{T}$  flips both spins:

$$\mathcal{T}: |\uparrow\rangle \leftrightarrow |\downarrow\rangle, \quad f_\sigma \rightarrow \sigma_{\sigma\sigma'}^y f_{\sigma'}, \quad \mathbf{i} \rightarrow -\mathbf{i}. \quad (4)$$

Here,  $|\tau\rangle$ 's represent  $\theta$  field, which rotate  $\pm\pi$  when crossing an Ising domain wall along or against a directed bond. For the arrow configuration in Fig. 2, an Ising domain wall going through site  $(\mathbf{r}, u/v)$  leads to  $n_v = \pm 1$  at this site. To match  $n_v$ , fermions at site  $(\mathbf{r}, u/v)$  are holes or electrons. Therefore,

$$[n_f, f_{\mathbf{r},s,\sigma}] = -(-1)^s f_{\mathbf{r},s,\sigma}, \quad (5)$$

where  $(-1)^s = \pm 1$  for  $s = u/v$ . The fermion spin is enforced to follow the majority Ising spins at adjacent plaquettes, as shown in Fig. 2. With such majority rule as well as Eq. (4), one can check that

$$\mathcal{T}|\psi_c\rangle = (-1)^{N_{\text{dw}}(c)} |\psi_{\mathcal{T}c}\rangle, \quad (6)$$

where  $c$  labels an Ising spin configuration,  $|\psi_c\rangle$  the corresponding decorated fermion state, and  $N_{\text{dw}}$  the number of domain wall loops in  $c$ .

The fixed-point wave function is expressed as [24]

$$|\Psi\rangle = \sum_c \Psi(c) |c\rangle \otimes |\psi_c\rangle, \quad (7)$$

where  $\Psi(c) = \pm 1$  satisfies  $\Psi(c) = (-1)^{N_{\text{dw}}(c)} \Psi(\mathcal{T}c)$  [42].

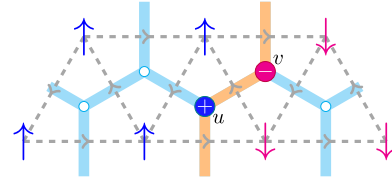


FIG. 2. Configuration of the QSH phase's fixed-point wave function.  $f_\sigma$  occupy the honeycomb lattice, while  $|\tau\rangle$  on the dual lattice. Crossing an Ising domain wall along or against oriented bonds of the dual lattice introduces a  $\pm\pi$  phase shift. Spins of fermions adhere to the majority rule.

*Tensor network representation.*—Constructing variational wave functions beyond Eq. (7) is highly desirable for practical purposes. We now present a comprehensive framework based on fPEPS. These are constructed by fermionic tensors, which are quantum states residing in the fermionic tensor product ( $\otimes_f$ ) of physical and internal legs. The legs with inward and outward arrows correspond to fermionic Hilbert spaces of ket and bra states, respectively. Fermionic tensor contraction fTr are implemented by connecting outward and inward internal legs, defined as

$$\text{fTr}[|i\rangle \otimes_f |j\rangle] = (-1)^{|i||j|} \text{fTr}[|j\rangle] \otimes_f \langle i| = \delta_{ij}, \quad (8)$$

where  $(-1)^{|i|}$  ( $|i| = 0/1$ ) is the fermion parity of  $|i\rangle$ . Physical wave functions are obtained by contracting all internal legs. Site and bond tensors for fPEPS on honeycomb lattice are drawn in Fig. 3, where all tensors are set to be *parity even* in this Letter. More details about fPEPS are represented in Sec. I of Supplemental Material (SM) [43].

Let us derive fPEPS representation of Eq. (7). Imposing translational symmetry, we focus on local tensors in a

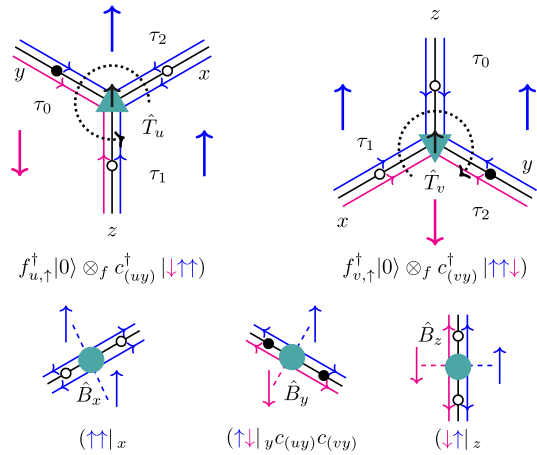


FIG. 3. Site tensors  $\hat{T}_{u,v}$  and bond tensors  $\hat{B}_{x,y,z}$ . Physical spin-1/2 fermions live at sites, while physical Ising spins live at bonds. Internal legs are represented by triple lines. Lines on two sides are internal Ising spins  $|\tau_0\tau_1\rangle$ , whose order follows the dashed arcs. The middle line is a spinless fermion  $c$ , where filled and empty circles label filled and empty states.

single unit cell, including site tensors  $\hat{T}_{u,v}$  and bond tensors  $\hat{B}_{x,y,z}$ , as illustrated in Fig. 3. Physical fermions live at sites, while two physical Ising spins live at two sides of bonds. Ising spins within a plaquette are enforced to be the same, effectively living at plaquette centers.

An internal leg ( $s\alpha$ ) is depicted as a triple line, pointing from site  $s$  to bond  $\alpha$ , with the middle line a spinless fermion mode  $c_{(s\alpha)}$ , and lines at sides Ising spins. Basis states are

$$\begin{aligned}\hat{T}_u &= |0\rangle \otimes_f [|\uparrow\uparrow\uparrow\rangle + |\downarrow\downarrow\downarrow\rangle] + f_{u,\uparrow}^\dagger |0\rangle \otimes_f [c_{(ux)}^\dagger |\uparrow\uparrow\downarrow\rangle + c_{(uz)}^\dagger |\uparrow\downarrow\uparrow\rangle + c_{(uy)}^\dagger |\downarrow\uparrow\uparrow\rangle] \\ &\quad + f_{u,\downarrow}^\dagger |0\rangle \otimes_f [-c_{(uy)}^\dagger |\downarrow\downarrow\uparrow\rangle + c_{(ux)}^\dagger |\downarrow\uparrow\downarrow\rangle - c_{(uz)}^\dagger |\uparrow\downarrow\downarrow\rangle] \\ \hat{T}_v &= |0\rangle \otimes_f [|\uparrow\uparrow\uparrow\rangle + |\downarrow\downarrow\downarrow\rangle] + f_{v,\uparrow}^\dagger |0\rangle \otimes_f [c_{(vy)}^\dagger |\uparrow\uparrow\downarrow\rangle + c_{(vx)}^\dagger |\uparrow\downarrow\uparrow\rangle + c_{(vz)}^\dagger |\downarrow\uparrow\uparrow\rangle] + f_{v,\downarrow}^\dagger |0\rangle \\ &\quad \otimes_f [c_{(vx)}^\dagger |\downarrow\downarrow\uparrow\rangle - c_{(vz)}^\dagger |\downarrow\uparrow\downarrow\rangle + c_{(vy)}^\dagger |\uparrow\downarrow\downarrow\rangle].\end{aligned}\quad (9)$$

Similarly,  $\langle\tau_0\tau_1|$  represents a bond spin state  $\langle\tau_0\tau_1|_\alpha \otimes (\tau_0\tau_1|_{(u\alpha)}(\tau_1\tau_0|_{(v\alpha)})$ , and we have

$$\hat{B}_\alpha = \langle\uparrow\uparrow|_\alpha + \langle\downarrow\downarrow|_\alpha + \langle\downarrow\uparrow|_\alpha - \langle\uparrow\downarrow|_\alpha c_{(u\alpha)}c_{(v\alpha)}. \quad (10)$$

As shown in Sec. II of SM [43], two  $\mathcal{T}$ -related state from contracting fPEPS satisfy Eq. (6), so it indeed gives the same fixed-point wave function.

*Tensor equations.*—To proceed, we extract symmetry action rules on internal legs for Eqs. (9) and (10), which pave the way for wave functions beyond Eq. (7). We assume that symmetries on physical legs can be pushed to gauge transformation on internal legs [44]; see also SM [43].

One way to impose charge conservation is to set all tensors charge neutral, which can be realized by assigning  $c_{(s\alpha)}$  to carry charge  $(-1)^{1-s}$ . Note that  $f_{s,\sigma}$  carries charge  $(-1)^s$ , and thus

$$\left(n_{f;s} + \sum_{\alpha=x,y,z} n_{f;(s\alpha)}\right) \cdot \hat{T}_s = \hat{B}_\alpha \cdot \left(\sum_{s=u,v} n_{f;(s\alpha)}\right) = 0.$$

$\mathcal{T}$  action on  $(s\alpha)$  are set as

$$\begin{aligned}W_{(s\alpha)}(\mathcal{T}) &= |\uparrow\uparrow\rangle_{(s\alpha)} (\downarrow\downarrow|_{(s\alpha)} + |\downarrow\downarrow\rangle_{(s\alpha)}) (\uparrow\uparrow|_{(s\alpha)}) \\ &\quad + i c_{(s\alpha)}^\dagger |\uparrow\downarrow\rangle_{(s\alpha)} (\downarrow\uparrow|_{(s\alpha)} + |\downarrow\uparrow\rangle_{(s\alpha)}) (\uparrow\downarrow|_{(s\alpha)}) c_{(s\alpha)},\end{aligned}\quad (11)$$

which leads to following equations:

$$\begin{aligned}\hat{T}_s &= U_s(\mathcal{T}) \otimes_f W_{(sx)}(\mathcal{T}) \otimes_f W_{(sy)}(\mathcal{T}) \otimes_f W_{(sz)}(\mathcal{T}) \cdot \hat{T}_s^*, \\ \hat{B}_\alpha &= V_{(\alpha 0)}(\mathcal{T}) \otimes_f V_{(\alpha 1)}(\mathcal{T}) \cdot \hat{B}_\alpha^* \cdot W_{(v\alpha)}^{-1}(\mathcal{T}) \otimes_f W_{(u\alpha)}^{-1}(\mathcal{T}).\end{aligned}$$

Here,  $U(\mathcal{T})$  and  $V(\mathcal{T})$  are  $\mathcal{T}$  action on physical fermions and Ising spins. We mention that, as  $W(\mathcal{T})$ 's are not parity

$(c_{(s\alpha)}^\dagger)^n |\tau_0\tau_1\rangle_{(s\alpha)}$ , where vacuum  $|0\rangle_{(s\alpha)}$  is omitted for brevity.  $\tau_0\tau_1$  are ordered counterclockwise and clockwise around the site  $u/v$ , as indicated by directed dashed arcs in Fig. 3.

As spins are identical within a plaquette, an internal spin state of a site tensor is  $|\tau_1\tau_2\rangle_{(sx)} |\tau_2\tau_0\rangle_{(sy)} |\tau_0\tau_1\rangle_{(sz)}$ , which is shortened as  $|\tau_0\tau_1\tau_2\rangle$ . Site tensors for Eq. (7) are

even, it may not give a symmetric wave function. In SM [43] Sec. III, we show that the above equations contain a hidden Kasteleyn orientation [19,20,45,46], which indeed leads to a  $\mathcal{T}$ -symmetric condition.

Besides the above physical symmetries, local tensors also host a ‘‘gauge symmetry’’ due to identical internal spins within a plaquette:

$$\begin{aligned}(n_{\lambda;(s\alpha 0)} + n_{\lambda;(s\bar{\alpha} 1)}) \cdot \hat{T}_s &= 0, \\ \hat{B}_\alpha \cdot (n_{\lambda;(u\alpha\alpha)} + n_{\lambda;(v\alpha\alpha)}) &= 0,\end{aligned}\quad (12)$$

where  $n_{\lambda;(s\alpha a)} = (-1)^{s+a} |\downarrow\rangle\langle\downarrow|$  with  $a = 0/1$  labeling two side lines of  $(s\alpha)$ , and  $\bar{\alpha} \equiv \alpha - (-1)^s$ .  $n_\lambda$ 's action within a plaquette  $p$  generates a  $U(1)$  symmetry. We thus get  $[U(1)]^{N_p}$  symmetry, where  $N_p$  is the number of plaquettes. Note that such symmetry acts trivially on physical legs, and is called ‘‘invariant gauge group’’ (IGG) [47–49], which is essential for topological ordered phases [50] as well as SPT phases [29,52,53].

We now extract relations between  $n_f$ ,  $W(\mathcal{T})$ , and  $n_\lambda$ , which are coined as ‘‘tensor equations’’ in this Letter. Roughly speaking, IGG gives possible action of the identity element on internal legs, and then symmetry on internal legs satisfy Eq. (1) up to some IGG element [47–49]. From Eq. (11), the commutator between  $n_f$  and  $\mathcal{T}$  on internal legs reads

$$W_{(s\alpha)}(\mathcal{T}) \cdot n_{f;(s\alpha)} \cdot W_{(s\alpha)}^{-1}(\mathcal{T}) = n_{f;(s\alpha)} + n_{D;(s\alpha)}, \quad (13)$$

where

$$\begin{aligned}n_{D;(s\alpha)} &= (-1)^s (|\downarrow\uparrow\rangle\langle\downarrow\uparrow| - |\uparrow\downarrow\rangle\langle\uparrow\downarrow|) \\ &= n_{\lambda;(s\alpha 0)} + n_{\lambda;(s\alpha 1)}.\end{aligned}\quad (14)$$

Physically,  $n_D$  gives  $U(1)$  gauge theory, but due to the decomposition to  $n_\lambda$ 's, such gauge theory is killed [54], leading to short-range entangled phase [43].

For group relation  $\mathcal{T}^2 = F$ , from Eqs. (11) and (14), we have

$$\exp\left[i\frac{\pi}{2}n_{D;(s\alpha)}^2\right] \cdot W_{(s\alpha)}(\mathcal{T}) \cdot W_{(s\alpha)}^*(\mathcal{T}) = F_{(s\alpha)}, \quad (15)$$

which is distinct from a naïve insertion of an IGG element. This is explained in detail in Sec. IV of SM [43].

The commutator between  $W(\mathcal{T})$  and  $n_\lambda$  completes tensor equations

$$W_{(s\alpha)}(\mathcal{T}) \cdot n_{\lambda;(s\alpha)}^* \cdot W_{(s\alpha)}^{-1}(\mathcal{T}) = -n_{\lambda;(s\alpha)} + (-)^{s+a}. \quad (16)$$

*Edge theories from tensor equations.*—In the following, we show that anomalous properties of edge can be extracted from Eq. (13) to Eq. (16).

We claim that edge anomaly can be detected through fusion of  $\mathcal{T}$  flux [55]. To see this, let us turn back to the interacting edge theory in Eq. (2).  $\mathcal{T}$  flux at  $x_{0,1}$  is created by  $\mathcal{T}$  action on  $x_0 \leq x \leq x_1$  [56], which also rotates  $\theta(x)$  by  $\pi$  within this segment (see Appendix A). Since  $j = \partial_i\theta/2\pi$ , a unit charge will be pumped from  $x_0$  to  $x_1$  by  $2\pi$  rotation of  $\theta$  [57,58], which is interpreted as *two  $\mathcal{T}$  flux fuses to an electron or hole*.

We now extract such fusion rule from tensor equations. As in Fig. 4, to obtain edge theory of system  $A$ , we cut tensors within  $A$  from the infinite fPEPS, contract all internal legs within  $A$ , and obtain a large tensor  $\hat{T}_A$ .  $\hat{T}_A$  has  $L$  boundary legs labeled by index  $j \in \partial A = \{1, 2, \dots, L\}$ , forming Hilbert space  $\mathbb{H}_{\partial A}$ . As shown in Sec. V of SM [43], the edge Hilbert spaces  $\mathbb{H}_{\text{edge}}$  are formed by states in  $\mathbb{H}_{\partial A}$  that are invariant under IGG action. Let  $P_{\text{edge}}$  be the projector from  $\mathbb{H}_{\partial A}$  to  $\mathbb{H}_{\text{edge}}$ . In our case,  $P_{\text{edge}}$  identifies Ising spins belonging to the same plaquette:  $\tau_{j+\frac{1}{4}} = \tau_{j+\frac{3}{4}}$ , where  $\tau_{j\pm\frac{1}{4}}$  are spins at boundary leg  $j$ .

By projecting  $W_{\partial A}(\mathcal{T}) \equiv \otimes_{f;j \in \partial A} W_j(\mathcal{T})$  to  $\mathbb{H}_{\text{edge}}$ , one gets  $\mathcal{T}$  action on edge

$$U_{\text{edge}}(\mathcal{T})\mathcal{K} = W_{\partial A}(\mathcal{T})\mathcal{K} \cdot P_{\text{edge}}. \quad (17)$$

Let  $M = \{2, 3, \dots, l\}$  be a subregion of  $\partial A$ .  $\mathcal{T}$  flux at ends of  $M$  are created by a charge-neutral string operator  $U_M(\mathcal{T})\mathcal{K}$ , where

$$U_M(\mathcal{T})\mathcal{K} = P_{\text{edge}} \cdot w_{l+1} \cdot w_1 \cdot W_M(\mathcal{T})\mathcal{K} \cdot P_{\text{edge}}. \quad (18)$$

Here,  $w_{1/(l+1)}$  are local operators on leg  $1/(l+1)$ . The charge-neutral requirement for  $U_M(\mathcal{T})\mathcal{K}$  puts the following constraint on  $w_{1/(l+1)}$  [43]:

$$[w_1, n_{f;1}] = n_{\lambda;\frac{3}{2}}^{(0)} \cdot w_1; \quad [w_{l+1}, n_{f;l+1}] = n_{\lambda;l+\frac{1}{2}}^{(1)} \cdot w_{l+1}, \quad (19)$$

with  $n_{\lambda;p}^{(0/1)}$  IGG elements acting on  $|\tau_{p\mp\frac{1}{4}}\rangle$ .

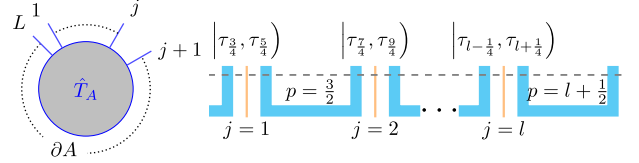


FIG. 4. Left: tensor  $\hat{T}_A$  cutting from the infinite fPEPS, whose boundary legs are numbered from 1 to  $L$ . Right: boundary leg  $j$  is a triple line, representing two Ising spins (thick blue line)  $\tau_{j-\frac{1}{4}}$  and  $\tau_{j+\frac{1}{4}}$ , and one spinless fermion  $c_j$  (thin orange line). Plaquettes between  $j$  and  $j+1$  are labeled as  $p = j + \frac{1}{2}$ .

Let  $j = 1$  and  $l+1$  be  $v$  site, then we have

$$\begin{aligned} w_1 &= \sum_{\tau_{\frac{3}{4}}} c_1 |\tau_{\frac{3}{4}}, \downarrow_{\frac{5}{4}}\rangle (\tau_{\frac{3}{4}}, \uparrow_{\frac{1}{4}} | + |\tau_{\frac{3}{4}}, \uparrow_{\frac{1}{4}}\rangle (\tau_{\frac{3}{4}}, \downarrow_{\frac{5}{4}} |); \\ w_{l+1} &= \sum_{\tau_{l+\frac{5}{4}}} c_{l+1}^{\dagger} |\downarrow_{l+\frac{3}{4}}, \tau_{l+\frac{5}{4}}\rangle (\uparrow_{l+\frac{3}{4}}, \tau_{l+\frac{5}{4}} | \\ &\quad + |\uparrow_{l+\frac{3}{4}}, \tau_{l+\frac{5}{4}}\rangle (\downarrow_{l+\frac{3}{4}}, \tau_{l+\frac{5}{4}} |). \end{aligned} \quad (20)$$

It is then straightforward to verify

$$[U_M(\mathcal{T})\mathcal{K}]^2 = P_{\text{edge}} \cdot \Omega_1 \cdot \Omega_{l+1} \cdot \prod_{j=2}^l F_j \cdot P_{\text{edge}}, \quad (21)$$

where  $\Omega_1 = c_1 \exp[i(\pi/2) \cdot n_{\lambda;\frac{3}{2}}^{(0)}]$  is a hole, and  $\Omega_{l+1} = c_{l+1}^{\dagger} \exp[i(\pi/2) \cdot n_{\lambda;l+\frac{1}{2}}^{(1)}]$  an electron (see details in SM, Sec. VI [43]). We thus recover the anomalous properties of edge, which suggests that any fPEPS that satisfies tensor equations belongs to the QSH phase [59].

*Variational tensor wave functions.*—The fixed-point wave function in Eq. (7) requires plaquette Ising spins, which is unusual in realistic models. Here, we construct variational tensor wave functions for spin-1/2 fermions on a honeycomb lattice. We will further demonstrate these wave functions belong to the QSH phase by calculating many-body topological invariants in the next part.

We start from translational invariant honeycomb fPEPS, whose site tensor is expressed as  $\hat{T}_s = (T_s)_{ijk,p} |p\rangle_s |i\rangle_{(sx)} |j\rangle_{(sy)} |k\rangle_{(sz)}$ , with  $s = u/v$  labeling sublattices, and  $(sx)$  to  $(sz)$  labeling internal legs. Physical spin-1/2 fermions  $f_{s\sigma}$ 's carry opposite charges on site  $u$  and  $v$ . For simplicity, we choose basis states of an internal leg  $(s\alpha)$  to be  $\{|\uparrow\uparrow\rangle_{(s\alpha)}, c_{(s\alpha)}^{\dagger} |\uparrow\downarrow\rangle_{(s\alpha)}, |\downarrow\uparrow\rangle_{(s\alpha)}, |\downarrow\downarrow\rangle_{(s\alpha)}\}$ .

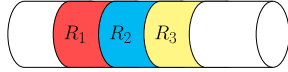
Action of  $\mathcal{T}$  on physical legs follows Eq. (4). Symmetries impose constraints on site tensor  $\hat{T}_s$  as

$$\begin{aligned} \otimes_{\alpha=x}^z W_{(s\alpha)}(\mathcal{T}) \otimes_f U_s(\mathcal{T}) \cdot \hat{T}_s^* &= \hat{T}_s \\ \left[ \sum_{\alpha=x}^z n_{f;(s\alpha)} + n_{f;s} \right] \cdot \hat{T}_s &= 0. \end{aligned} \quad (22)$$



In addition, site tensors should also be invariant under plaquette IGG  $n_\lambda$ 's, as in Eq. (12).  $W(\mathcal{T})$ ,  $n_f$ , and  $n_\lambda$  satisfy tensor equations from Eqs. (13) to (16), and can simply take the same form as in the previous example. By solving these tensor constraints, we obtain seven linearly independent solutions for  $\hat{T}_{u/v}$ , as listed in Appendix B. Bond tensors are set to be Eq. (10), which satisfy all tensor equations [43]. We also calculated the variational ansatz for system in square lattice; see SM [43].

*Many-body topological invariants.*—The correlated QSH wave function can be detected by the many-body topological invariant proposed in Ref. [37]. The system is put on a cylinder periodic in  $y$  direction and open in  $x$  direction, which is divided as follows



The topological invariant is given by

$$Z = \text{Tr}[\rho_{R_1 \cup R_3}^+ C_T^{R_1} (\rho_{R_1 \cup R_3}^-)^{T_1} [C_T^{R_1}]^\dagger] \quad (23)$$

with

$$\rho_{R_1 \cup R_3}^\pm = \text{Tr}_{R_1 \cup R_3} \left[ \exp \frac{\pm 2\pi i \sum_{r \in R_2} y n(r)}{L_y} |\Phi\rangle \langle \Phi| \right].$$

Here,  $T_1$  is the fermionic partial transpose of region  $R_1$ , and  $C_T^{R_1}$  is defined by  $C_T^{R_1} c_{j \in R_1} (C_T^{R_1})^\dagger = c_{k \in R_1}^\dagger U(\mathcal{T})_{kj}$ . The phase of  $Z$  takes value  $0/\pi$  when  $|\Phi\rangle$  represents a trivial or topological insulator. This quantity is computed numerically, and certain outcomes are depicted in Fig. 5. Notably, for local tensors that satisfy the tensor equations characterizing the QSH phase,  $\text{sgn}(Z) = -1$  is realized within a finite parameter region. It is noteworthy that the occurrence of  $\text{sgn}(Z) = 1$  in other parameter regions may be attributed to diverse factors, such as finite size effects. Further details are provided in SM [43].

*Discussion.*—In this Letter, we extract tensor equations from the fPEPS representation of the QSH fixed-point

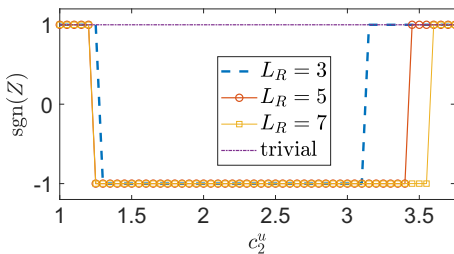


FIG. 5. Calculation of  $\text{sgn}(Z)$  for ansatz of trivial or topological insulators. Here,  $c_2^u$  denotes some variational parameters for local tensors, which satisfy tensor equations for the QSH phase. See Appendix B for details. Sizes of  $R_{1,2,3}$  are set to be equal, with length in  $x$  direction to be  $L_R$ , and in  $y$  direction to be 2.

wave function, as detailed in Eqs. (13) to (16). Through a systematic solution of these tensor equations, we obtain general forms for symmetry operations on the internal legs of fPEPS. Utilizing the obtained symmetry constraints on the local tensors, we construct generic variational tensor wave functions for the QSH phase, which is verified by numerically extracting topological invariants for many-body systems.

This Letter leaves several interesting future directions. First, to express variational ansatz for topological phases in half-filled spin-1/2 *electronic* models, it is necessary to generalize our framework to include tensors with odd parity. Additionally, developing variational numerical algorithms for symmetric fPEPS wave functions obtained in this Letter would be desirable to simulate the QSH phase in strongly correlated models. On the analytical side, we aim to explore other fermionic topological phases, such as topological superconductors and topologically ordered phases. Of particular interest is the investigation of chiral phases, such as the  $p + ip$  topological superconductor [61–63]. The question of whether fPEPS can accurately represent these chiral phases with a finite bulk gap remains an intriguing puzzle [64–66]. Furthermore, tensor networks readily incorporate spatial symmetries [48], enabling the construction of variational tensor wave functions for gapped electronic liquid phases and high-order topological insulators or superconductors [67–69]. Exploring these possibilities holds significant potential for advancing our understanding of exotic topological phases.

We would like to thank Qing-Rui Wang and Xie Chen for helpful discussions. The work is supported by MOST No. 2022YFA1403902, NSFC No. 12104451, CAS under Contract No. JZHKYPT-2021-08, and funds from Strategic Priority Research Program of CAS (No. XDB28000000).

*Appendix A: Interacting edge theory.*—In the free fermion case, the anomalous edge states of the QSH phase are described by massless helical Dirac fermions:

$$H_{\text{edge}} = \int dx (-iv_F) [\psi_R^\dagger(x) \partial_x \psi_R(x) - \psi_L^\dagger(x) \partial_x \psi_L(x)],$$

where  $\psi_{L/R}$  is the left and right moving fermion mode, and  $v_F$  the fermion velocity.  $\mathcal{T}$  acts as  $\psi_{R/L} \rightarrow \pm i \psi_{L/R}$ , forbidding mass terms opening a gap.

The interacting edge theory can be analyzed by the bosonization method [38]. Conjugate fields  $\phi(x)$  and  $\theta(x)$  are introduced, both with periodicity  $2\pi$ , where  $[\partial_x \theta(x), \phi(x')] = 2\pi i \delta(x - x')$ . With these hydrodynamic variables,  $\psi_{R/L}(x) \sim \exp[-(i\phi(x) \pm i\theta(x)/2)]$ , charge density  $\delta\rho(x) = -\partial_x \theta(x)/2\pi$ , and current density  $j(x) = \partial_x \phi(x)/2\pi$ . Symmetry actions on  $\theta$  and  $\phi$  listed in Eq. (3) are derived from its action on  $\psi_{R/L}$ . Lagrangian density for the interacting edge theory is [34,35]

$$\mathcal{L}_{\text{edge}} = \frac{1}{2\pi} \partial_x \theta \partial_t \phi - \frac{v_F}{4\pi} \left( \frac{1}{K} (\partial_x \theta)^2 + K (\partial_x \phi)^2 \right) + \alpha \cos(2\theta - 2\theta_0), \quad (\text{A1})$$

where  $K$  is the Luttinger parameter, and for the noninteracting case  $K = 2$ . Because of Eq. (3), the leading relevant symmetric scattering term is  $\alpha \cos(2\theta - 2\theta_0)$  with scaling dimension  $2K$ . It becomes relevant when  $K < 1$ , driving edge to a gapped phase. For the case where  $\alpha > 0$ , such gapped phase has doubly degenerate ground states, characterized by  $\langle \theta \rangle = \theta_0$  and  $\langle \theta \rangle = \theta_0 + \pi$ , respectively, both minimizing  $\alpha \cos(2\theta - 2\theta_0)$ . The two ground states are exchanged under  $\mathcal{T}$ , and thus spontaneously break  $\mathcal{T}$  symmetry.

Topological defects of this  $\mathcal{T}$ -breaking phase host anomalous properties. We consider a time reversal domain wall at  $x_0$ , with domains  $\langle \theta(x < x_0 - \epsilon) \rangle = \theta_0$  and  $\langle \theta(x > x_0 + \epsilon) \rangle = \theta_0 + \pi$ , as shown in Fig. 1. For region  $(x_0 - \epsilon, x_0 + \epsilon)$ ,  $\theta$  rotate clockwise or counterclockwise. Such domain wall carries  $\pm 1/2$  charge [39], as

$$\int_{x_0-\epsilon}^{x_0+\epsilon} dx \delta\rho(x) = \int_{x_0-\epsilon}^{x_0+\epsilon} dx \left( -\frac{\partial_x \theta(x)}{2\pi} \right) = \pm \frac{1}{2}. \quad (\text{A2})$$

*Appendix B: Numerical details.*—Here, we present the variation ansatz solved from Eq. (22) and used for calculating the many-body topological invariant. The  $u/v$ -sublattice variational site tensor  $\hat{T}_{u/v} = \sum_l c_l^{u/v} t_l^{u/v}$  is a linear combination of component tensors  $t_l^{u/v}$ , with real coefficients  $c_l^{u/v}$ 's. Component tensors are listed below:

$$\begin{aligned} t_1^u &= \begin{array}{c} \uparrow \\ \downarrow \\ \uparrow \\ \downarrow \end{array} + \begin{array}{c} \downarrow \\ \uparrow \\ \downarrow \\ \uparrow \end{array}; t_2^u = \begin{array}{c} \uparrow \\ \downarrow \\ \uparrow \\ \downarrow \end{array} - \begin{array}{c} \downarrow \\ \uparrow \\ \downarrow \\ \uparrow \end{array}; \\ t_3^u &= \begin{array}{c} \uparrow \\ \downarrow \\ \uparrow \\ \downarrow \end{array} + \begin{array}{c} \downarrow \\ \uparrow \\ \downarrow \\ \uparrow \end{array}; t_4^u = \begin{array}{c} \uparrow \\ \downarrow \\ \uparrow \\ \downarrow \end{array} + \begin{array}{c} \downarrow \\ \uparrow \\ \downarrow \\ \uparrow \end{array}; \\ t_5^u &= \begin{array}{c} \uparrow \\ \downarrow \\ \uparrow \\ \downarrow \end{array} - \begin{array}{c} \downarrow \\ \uparrow \\ \downarrow \\ \uparrow \end{array}; t_6^u = \begin{array}{c} \uparrow \\ \downarrow \\ \uparrow \\ \downarrow \end{array} - \begin{array}{c} \downarrow \\ \uparrow \\ \downarrow \\ \uparrow \end{array}; \\ t_7^u &= \begin{array}{c} \uparrow \\ \downarrow \\ \uparrow \\ \downarrow \end{array} + \begin{array}{c} \downarrow \\ \uparrow \\ \downarrow \\ \uparrow \end{array}; t_7^v = \begin{array}{c} \uparrow \\ \downarrow \\ \uparrow \\ \downarrow \end{array} - \begin{array}{c} \downarrow \\ \uparrow \\ \downarrow \\ \uparrow \end{array}; \\ t_1^v &= \begin{array}{c} \uparrow \\ \downarrow \\ \uparrow \\ \downarrow \end{array} + \begin{array}{c} \downarrow \\ \uparrow \\ \downarrow \\ \uparrow \end{array}; t_2^v = \begin{array}{c} \uparrow \\ \downarrow \\ \uparrow \\ \downarrow \end{array} + \begin{array}{c} \downarrow \\ \uparrow \\ \downarrow \\ \uparrow \end{array}; \\ t_3^v &= \begin{array}{c} \uparrow \\ \downarrow \\ \uparrow \\ \downarrow \end{array} - \begin{array}{c} \downarrow \\ \uparrow \\ \downarrow \\ \uparrow \end{array}; t_4^v = \begin{array}{c} \uparrow \\ \downarrow \\ \uparrow \\ \downarrow \end{array} - \begin{array}{c} \downarrow \\ \uparrow \\ \downarrow \\ \uparrow \end{array}; \\ t_5^v &= \begin{array}{c} \uparrow \\ \downarrow \\ \uparrow \\ \downarrow \end{array} + \begin{array}{c} \downarrow \\ \uparrow \\ \downarrow \\ \uparrow \end{array}; t_6^v = \begin{array}{c} \uparrow \\ \downarrow \\ \uparrow \\ \downarrow \end{array} + \begin{array}{c} \downarrow \\ \uparrow \\ \downarrow \\ \uparrow \end{array}. \end{aligned}$$

Here, dashed legs are fermion parity odd. For the trivial symmetric wave function used for benchmark, the first

component tensors for  $u/v$  sublattices are identical to  $t_1^u$  and  $t_1^v$  above. The others are listed below. The trivial symmetric solutions are solved under the same constraints as the QSH case, except Eq. (13). We show how to solve these constraints in SM [43].

$$\begin{aligned} t_2^u &= \begin{array}{c} \uparrow \\ \downarrow \\ \uparrow \\ \downarrow \end{array} + \begin{array}{c} \downarrow \\ \uparrow \\ \downarrow \\ \uparrow \end{array}; t_3^u = \begin{array}{c} \uparrow \\ \downarrow \\ \uparrow \\ \downarrow \end{array} + \begin{array}{c} \downarrow \\ \uparrow \\ \downarrow \\ \uparrow \end{array}; \\ t_4^u &= \begin{array}{c} \uparrow \\ \downarrow \\ \uparrow \\ \downarrow \end{array} + \begin{array}{c} \downarrow \\ \uparrow \\ \downarrow \\ \uparrow \end{array}; t_4^v = \begin{array}{c} \uparrow \\ \downarrow \\ \uparrow \\ \downarrow \end{array} + \begin{array}{c} \downarrow \\ \uparrow \\ \downarrow \\ \uparrow \end{array}; \\ t_2^v &= \begin{array}{c} \uparrow \\ \downarrow \\ \uparrow \\ \downarrow \end{array} + \begin{array}{c} \downarrow \\ \uparrow \\ \downarrow \\ \uparrow \end{array}; t_3^v = \begin{array}{c} \uparrow \\ \downarrow \\ \uparrow \\ \downarrow \end{array} + \begin{array}{c} \downarrow \\ \uparrow \\ \downarrow \\ \uparrow \end{array}. \end{aligned}$$

\*Corresponding author: jiangsh@ucas.ac.cn

†Corresponding author: xuchao@ucas.ac.cn

- [1] C. L. Kane and E. J. Mele, *Phys. Rev. Lett.* **95**, 226801 (2005).
- [2] X.-L. Qi and S.-C. Zhang, *Rev. Mod. Phys.* **83**, 1057 (2011).
- [3] M. Z. Hasan and C. L. Kane, *Rev. Mod. Phys.* **82**, 3045 (2010).
- [4] X.-L. Qi, T. L. Hughes, and S.-C. Zhang, *Phys. Rev. B* **78**, 195424 (2008).
- [5] L. Fidkowski and A. Kitaev, *Phys. Rev. B* **81**, 134509 (2010).
- [6] L. Fidkowski and A. Kitaev, *Phys. Rev. B* **83**, 075103 (2011).
- [7] X. Chen, Z.-C. Gu, and X.-G. Wen, *Phys. Rev. B* **84**, 235128 (2011).
- [8] Z.-C. Gu and X.-G. Wen, *Phys. Rev. B* **90**, 115141 (2014).
- [9] Z.-C. Gu and M. Levin, *Phys. Rev. B* **89**, 201113(R) (2014).
- [10] Q.-R. Wang and Z.-C. Gu, *Phys. Rev. X* **8**, 011055 (2018).
- [11] Q.-R. Wang and Z.-C. Gu, *Phys. Rev. X* **10**, 031055 (2020).
- [12] C. Wang, C.-H. Lin, and Z.-C. Gu, *Phys. Rev. B* **95**, 195147 (2017).
- [13] M. Cheng, N. Tantivasadakarn, and C. Wang, *Phys. Rev. X* **8**, 011054 (2018).
- [14] C. Wang, A. C. Potter, and T. Senthil, *Science* **343**, 629 (2014).
- [15] C. Wang and T. Senthil, *Phys. Rev. B* **89**, 195124 (2014).
- [16] T. Senthil, *Annu. Rev. Condens. Matter Phys.* **6**, 299 (2015).
- [17] E. Witten, *Rev. Mod. Phys.* **88**, 035001 (2016).
- [18] D. S. Freed and M. J. Hopkins, *Geom. Topol.* **25**, 1165 (2021).
- [19] B. Ware, J. H. Son, M. Cheng, R. V. Mishmash, J. Alicea, and B. Bauer, *Phys. Rev. B* **94**, 115127 (2016).
- [20] N. Tarantino and L. Fidkowski, *Phys. Rev. B* **94**, 115115 (2016).
- [21] Z. Wang, S.-Q. Ning, and X. Chen, *Phys. Rev. B* **98**, 094502 (2018).
- [22] M. A. Metlitski, [arXiv:1908.08958](https://arxiv.org/abs/1908.08958).
- [23] J. H. Son and J. Alicea, *Phys. Rev. B* **100**, 155107 (2019).

- [24] Q.-R. Wang, Y. Qi, C. Fang, M. Cheng, and Z.-C. Gu, *Phys. Rev. B* **108**, L121104 (2023).
- [25] T. Barthel, C. Pineda, and J. Eisert, *Phys. Rev. A* **80**, 042333 (2009).
- [26] P. Corboz, G. Evenbly, F. Verstraete, and G. Vidal, *Phys. Rev. A* **81**, 010303(R) (2010).
- [27] C. V. Kraus, N. Schuch, F. Verstraete, and J. I. Cirac, *Phys. Rev. A* **81**, 052338 (2010).
- [28] Z.-C. Gu, F. Verstraete, and X.-G. Wen, [arXiv:1004.2563](https://arxiv.org/abs/1004.2563).
- [29] N. Schuch, D. Pérez-García, and I. Cirac, *Phys. Rev. B* **84**, 165139 (2011).
- [30] N. Bultinck, D. J. Williamson, J. Haegeman, and F. Verstraete, *J. Phys. A* **51**, 025202 (2017).
- [31] N. Bultinck, D. J. Williamson, J. Haegeman, and F. Verstraete, *Phys. Rev. B* **95**, 075108 (2017).
- [32] C. Wille, O. Buerschaper, and J. Eisert, *Phys. Rev. B* **95**, 245127 (2017).
- [33] J. I. Cirac, D. Perez-Garcia, N. Schuch, and F. Verstraete, *Rev. Mod. Phys.* **93**, 045003 (2021).
- [34] C. Wu, B. A. Bernevig, and S.-C. Zhang, *Phys. Rev. Lett.* **96**, 106401 (2006).
- [35] C. Xu and J. E. Moore, *Phys. Rev. B* **73**, 045322 (2006).
- [36] H. Shapourian, K. Shiozaki, and S. Ryu, *Phys. Rev. Lett.* **118**, 216402 (2017).
- [37] K. Shiozaki, H. Shapourian, K. Gomi, and S. Ryu, *Phys. Rev. B* **98**, 035151 (2018).
- [38] F. Haldane, *J. Phys. C* **14**, 2585 (1981).
- [39] J. Goldstone and F. Wilczek, *Phys. Rev. Lett.* **47**, 986 (1981).
- [40] X. Chen, Y.-M. Lu, and A. Vishwanath, *Nat. Commun.* **5**, 3507 (2014).
- [41] Z.-X. Liu, Z.-C. Gu, and X.-G. Wen, *Phys. Rev. Lett.* **113**, 267206 (2014).
- [42] We mention that to fully determine  $|\Psi\rangle$ , we should explicitly write down the fermion order and set the  $\pm 1$  phase for each  $\Psi(c)$ . However, we will not present such information as it is quite complicated and is unnecessary for the following discussion.
- [43] See Supplemental Material at <http://link.aps.org/supplemental/10.1103/PhysRevLett.132.126504> for a review of fermionic tensor network states, fixed-point wave function of QSH states, the Kasteleyn orientations for global symmetry constraints, detailed explanation of edge theories, and the example of variational ansatz calculation.
- [44] D. Pérez-García, M. Sanz, C. Gonzalez-Guillen, M. M. Wolf, and J. I. Cirac, *New J. Phys.* **12**, 025010 (2010).
- [45] D. Cimasoni and N. Reshetikhin, *Commun. Math. Phys.* **275**, 187 (2007).
- [46] T. D. Ellison and L. Fidkowski, *Phys. Rev. X* **9**, 011016 (2019).
- [47] X.-G. Wen, *Phys. Rev. B* **65**, 165113 (2002).
- [48] S. Jiang and Y. Ran, *Phys. Rev. B* **92**, 104414 (2015).
- [49] S. Jiang and Y. Ran, *Phys. Rev. B* **95**, 125107 (2017).
- [50] For topological ordered phases, the necessary symmetry conditions act purely on virtual legs (e.g., IGG symmetry constraints), and are invisible to physical degrees of freedom [51]. Such virtual symmetries characterize topological conservation of anyon excitations.
- [51] X. Chen, B. Zeng, Z.-C. Gu, I. L. Chuang, and X.-G. Wen, *Phys. Rev. B* **82**, 165119 (2010).
- [52] Z.-C. Gu, M. Levin, and X.-G. Wen, *Phys. Rev. B* **78**, 205116 (2008).
- [53] N. Schuch, I. Cirac, and D. Pérez-García, *Ann. Phys. (Amsterdam)* **325**, 2153 (2010).
- [54] Similar to topological ordered phases, SPT phases require IGG constraints. However, to avoid long-range entanglement, such IGG must be decomposable, as outlined in Eq. (14). Different from topological ordered phases, SPT phases always require a well-defined global physical symmetry.
- [55] D. V. Else and C. Nayak, *Phys. Rev. B* **90**, 235137 (2014).
- [56] X. Chen and A. Vishwanath, *Phys. Rev. X* **5**, 041034 (2015).
- [57] X.-L. Qi, T. L. Hughes, and S.-C. Zhang, *Nat. Phys.* **4**, 273 (2008).
- [58] L. Fu and C. L. Kane, *Phys. Rev. B* **74**, 195312 (2006).
- [59] It is possible that additional IGG elements emerge in the thermodynamic limit [60]. In such case, fPEPS wave function may give other phases, such as spontaneously symmetry breaking phases.
- [60] H. Dreyer, L. Vanderstraeten, J.-Y. Chen, R. Verresen, and N. Schuch, [arXiv:2008.04833](https://arxiv.org/abs/2008.04833).
- [61] N. Read and D. Green, *Phys. Rev. B* **61**, 10267 (2000).
- [62] D. A. Ivanov, *Phys. Rev. Lett.* **86**, 268 (2001).
- [63] M. Stone and R. Roy, *Phys. Rev. B* **69**, 184511 (2004).
- [64] T. B. Wahl, H.-H. Tu, N. Schuch, and J. I. Cirac, *Phys. Rev. Lett.* **111**, 236805 (2013).
- [65] T. B. Wahl, S. T. Haßler, H.-H. Tu, J. I. Cirac, and N. Schuch, *Phys. Rev. B* **90**, 115133 (2014).
- [66] J. Dubail and N. Read, *Phys. Rev. B* **92**, 205307 (2015).
- [67] A. Rasmussen and Y.-M. Lu, *Phys. Rev. B* **101**, 085137 (2020).
- [68] Z. Song, C. Fang, and Y. Qi, *Nat. Commun.* **11**, 1 (2020).
- [69] D. V. Else and R. Thorngren, *Phys. Rev. B* **99**, 115116 (2019).